Earthq Eng & Eng Vib (2020) 19: 903-917 **DOI**: https://doi.org/10.1007/s11803-020-0603-9

Seismic analysis of semi-sine shaped alluvial hills above subsurface circular cavity

Mehdi Panji† and Mohammad Habibivand‡

Department of Civil Engineering, Zanjan Branch, Islamic Azad University, Zanjan, Iran

Abstract: In this study, a seismic analysis of semi-sine shaped alluvial hills above a circular underground cavity subjected to propagating oblique SH-waves using the half-plane time domain boundary element method (BEM) was carried out. By dividing the problem into a pitted half-plane and an upper closed domain as an alluvial hill and applying continuity/boundary conditions at the interface, coupled equations were constructed and ultimately, the problem was solved step-by-step in the time domain to obtain the boundary values. After solving some verification examples, a semi-sine shaped alluvial hill located on an underground circular cavity was successfully analyzed to determine the amplification ratio of the hill surface. For sensitivity analysis, the effects of the impedance factor and shape ratio of the hill were also considered. The ground surface responses are illustrated as three-dimensional graphs in the time and frequency domains. The results show that the material properties of the hill and their heterogeneity with the underlying half-space had a significant effect on the surface response.

Keywords: alluvial semi-sine shaped hill; half-plane BEM; time domain; circular cavity; SH waves

1 Introduction

Site effects are one of the important factors that affect the amplitude of the responses during earthquakes on structures and lead to a growing interest among specialists in this field. The effects of surface topographic features including hills, valleys and subsurface openings, such as lined tunnels and underground cavities, or the combination of these topographies, on the amplification of the earthquake have been investigated in the literature as one of the major issues in the field of geotechnical engineering (Geli *et al*., 1988). Furthermore, the effects of heterogeneous materials and incident wave angle were considered as important factors on the response of the ground surface (Hadley, 1987). Therefore, efficient approaches to model these features have been developed. According to the technical literature, three main methodologies have been used including analytical, semi-analytical, and numerical methods (Sanchez-Sesma *et al*., 2002). In the analytical methods, special functions as well as appropriate equations are considered for each model of the topography, and boundary/initial conditions are accordingly applied. The responses obtained in these methods have been used by other researchers for benchmark purposes. For the first time, Sabina and Willis (1975) presented an analytical response in the frequency domain for different types of hills using the matched asymptotic expansion of the wave function. Many other studies have used these methods to solve the topographies problems, including Lee (1988), Yuan and Men (1992), Yuan and Liao (1996a & 1996b), Lin and Liu (2002), Wang and Liu (2002), Lee *et al*. (2004), Liang *et al*. (2005), Lee *et al*. (2006), Lu and Liu (2006), Tsaur and Chang (2009), Liang *et al*. (2010), Luo *et al*. (2010), Liang and Fu (2011), Amornwongpaibun and Lee (2013), Lee and Amornwongpaibun (2013),Yang *et al*. (2014), Zhang *et al*. (2015), Amornwongpaibun *et al*. (2015), Heather and Lee (2017), Zhang *et al*. (2018) and Liu *et al*. (2019). In addition, Liang *et al*. (2004), Liu *et al*. (2010) and Zhang *et al*. (2012) used the Bessel-Fourier function to solve the hill problems. Cao *et al*. (2001) also obtained an analytical response for a cylindrical hill by using the complex variable and conformal mapping methods. Qiu and Liu (2005) and Lin *et al*. (2010) used the complex function for a triangular hill problem.

On the other hand, semi-analytical approaches have been successfully developed to solve the hill problems. In the use of these methods, where the main part of the problem is analytically solved and the other part is analyzed numerically, Aki and Larner (1970) were able for the first time to present a method called "Aki-Larner" for analyzing a layered medium with irregular interface. Subsequently, Bouchon (1973), Bard (1982), and Geli *et al*. (1988) used the Aki-Larner method to study the hill topographies. Then, Datta (1974) and Sills (1978)

Correspondence to: Mehdi Panji, Department of Civil Engineering, Zanjan Branch, Islamic Azad University, Zanjan, Iran
Tel: +98-24-33421003-7; Fax: +98-24-33460463
E-mail: m.panji@iauz.ac.ir
†Assistant Professor; ‡MSc student
Received March 5, 2018; **Accepted** January 16, 2019

used semi-analytical techniques to analyze convex topographic problems. By combining the finite element method (FEM) and an analytical scheme, Data and Shah (1982) investigated the scattering of plane SH waves by subsurface circular cavities. Other semi-analytical methods used for analyzing the hill problems included the T-matrix method or the null-field approach (Chen *et al*., 2011 and 2012) and the Bouchon -Campillo method (Zhou and Chen, 2006).

In spite of presenting accurate responses, analytical and semi-analytical methods are not capable enough in modeling the anticipated topographic shapes that are compatible with those in nature. Therefore, numerical approaches have been developed for this purpose. In recent years, numerical methods have gained more interest from researchers, due to the advancements in computer science and their efficiency. Numerical methods for analyzing the topographic features are generally divided into three groups: volumetric, boundary and mixed methods (Sanchez Sesma *et al*., 2002). In volumetric methods, which frequently include the finite element method (FEM) and finite difference method (FDM), the whole body as well as surface of the model must be discretized. Therefore, they have an unavoidable significant computational cost. Smith (1975), Day (1977) and Luo *et al*. (2019) used the FEM to create topographic models in their research and Boor (1972, 1973), Virieux (1984) and Moczo (1989) used the FDM as the analyzing method. However, in the boundary element method (BEM), the volume of computations as well as the corresponding analysis time is low compared to the volumetric methods, due to the fact that only the boundary of the medium is discretized. The BEM can be formulated in two groups of the full-plane and half-plane (Dominguez and Meise, 1991); the dynamical studies that are carried out by these methods can be also formed in the frequency and time domains. In the full-plane BEM formulation, the entire boundaries of the model must be discretized including the surface topographic features plus a large part of the smooth ground surface in the sides of the zone of interest, and stress-free boundary conditions are approximately applied on the ground surface. Panji *et al*. (2011 and 2016) used full-plane BEM for analyzing the static stability of underground tunnels. In the field of dynamic studies, Sanchez-Sesma *et al*. (1982), Hadley (1987), Mogi and Kawakami (2007) and Ba *et al*. (2016 and 2017) used the full-plane BEM in the frequency domain, and the research of Takemia and Fujiwara (1994) and Kamalian *et al*. (2003, 2006 and 2008) was carried out by this method in the time domain.

In the use of half-plane BEM, only the boundary of the topography is discretized, considering that the stress-free boundary conditions on the smooth ground surface are completely and precisely satisfied in the governing equations. Therefore, the computational cost is significantly reduced compared to the full-plane case. Panji and Ansari (2017a) used half-plane BEM for static analysis of pressure pipes in a two-layer soil. There are also several researchers in the field of dynamic analysis who have conducted studies in the frequency domain; Wong and Jennings (1975), Sanchez-Sesma and Rosenblueth (1979), Sanchez-Sesma and Esquivel (1979), Dravinski (1980), Ohtsu and Uesugi (1985), Moeen-Vaziri and Trifunac (1988), Nowak and Hall (1993), Ding and Dravinski (1996), Ausilio *et al*. (2008) performed their studies by half-plane BEM in the frequency domain. Belytschko and Chang (1988) were the first to present the approach of the direct half-plane time domain BEM for seismic analysis of topographic features. Panji *et al*. (2013) proposed a simple procedure of half-plane time domain BEM to study the seismic topographies under SH-wave propagation. Panji *et al*. (2013) used this method for analyzing the topography of a 2D valley subjected to incident SH-waves. There are other studies that incorporated similar methods in their investigations, including seismic analysis of the homogeneous hill (Panji *et al*., 2014a), analyzing the semi-sine shaped valley located on an underground cavity (Panji *et al*., 2014b), the research carried out by Panji and Ansari (2017b) on the seismic analysis of lined tunnels, time history response on the surface in the presence of multiple cavities (Panji and Mojtabazadeh, 2018), transient response of irregular surfaces (Panji and Mojtabazadeh, 2020) and SH-wave scattering by subsurface inclusion (Panji *et al*., 2020) . To the best of the authors' knowledge, the problem of semi-sine shaped alluvial hills above underground circular cavities has not yet been analyzed in a straightforward way in the time domain.

In this study, a seismic analysis of alluvial semi-sine shaped hills located on an underground circular cavity was investigated subjected to propagating incident plane SH-waves using the half-plane time domain BEM. After developing the formulation of the method, the validation was performed by solving several practical examples in the analysis of similar combined topographies. Then, the response of an alluvial semi-sine shaped hill surface was sensitized by changing some key parameters of the model, such as the impedance factor and the shape ratio of the hill. The results are presented in terms of normalized displacement amplitude as well as amplification ratio and the figures are represented as three-dimensional diagrams in the time and frequency domains. One of the important goals of the present research is to observe the effect of heterogeneity of hill materials with underlying domain on the seismic response of the surface and present numerical results in graph form for use in seismic geotechnical studies.

2 Half-plane time domain BEM

The two-dimensional scalar wave equation in a linear elastic homogeneous domain and boundary condition on the smooth ground surface are presented as follows:

$$\frac{\partial^2 u(x,y,t)}{\partial x^2}+\frac{\partial^2 u(x,y,t)}{\partial y^2}+b(x,y,t)=\frac{1}{C^2}\frac{\partial^2 u(x,y,t)}{\partial t^2} \tag{1}$$

$$\frac{\partial u(x,y,t)}{\partial n}\Big|_{y=0}=0 \tag{2}$$

By solving Eq. (1) through the weighted residual integral method and applying the boundary conditions of Eq. (2), regardless of the body forces and the initial conditions, the boundary integral equation (BIE) in the time domain is obtained as follows (Brebbia and Dominguez, 1989; Dominguez, 1993):

$$c(\xi)u(\xi,t)=\int_{\Gamma}\cdot \left\{\int_0^t\left[u^*(x,t;\xi,\tau)q(x,\tau)-q^*(x,t;\xi,\tau)u(x,\tau)\right]\mathrm{d}\tau\right\}\mathrm{d}\Gamma(x)+u^{\mathrm{ff}}(\xi,t) \tag{3}$$

where u^* and q^* are the half-plane time domain displacement and traction fundamental solutions, respectively, which are obtained from the solution at point x and time t as a result of an out-of-plane impact force at position ξ and preceding time τ, as Eqs. (4) and (5). u and q are the displacement and traction fields on the boundary, respectively. $\Gamma(x)$ is the boundary of the domain and $c(\xi)$ is the coefficient of the shape. u^{ff} is the free-field displacement without surface irregularities.

$$u^*(x,t;\xi,\tau)=\frac{1}{2\pi}\left(\frac{H\left((t-\tau)-\frac{r}{C}\right)}{\sqrt{\left((t-\tau)^2-\left(\frac{r}{C}\right)^2\right)}}+\frac{H\left((t-\tau)-\frac{r'}{C}\right)}{\sqrt{\left((t-\tau)^2-\left(\frac{r'}{C}\right)^2\right)}}\right) \tag{4}$$

$$q^*(x,t;\xi,\tau)=\frac{C}{2\pi}\left(\left[\frac{rH\left[C(t-\tau)-r\right]}{\left[\sqrt{C^2(t-\tau)^2-r^2}\right]^3}\frac{\partial r}{\partial n}\right]+\left[\frac{r'H\left[C(t-\tau)-r'\right]}{\left[\sqrt{C^2(t-\tau)^2-r'^2}\right]^3}\frac{\partial r'}{\partial n}\right]\right) \tag{5}$$

in which r and r' are the distance from the source and image source to the receiver point and $H(..)$ is the Heaviside step function, and n and C are the normal vector of the surface and the shear wave velocity, respectively.

In order to solve Eq. (3) numerically in the time domain, the time axis and the boundary of geometry must be discretized. In this regard, an analytical process and a numerical scheme are considered for the first and second cases, respectively. To solve analytic time integral, the axis of time from 0 to t is discretized to N times with the length Δt ($\Delta t \times N = t$). Using the linear shape functions at each time step and removing the singular conditions of the wave, Eq. (3) is rewritten as follows:

$$c(\xi)u^N(\xi)=\sum_{n=1}^{N}\int_{\Gamma}\begin{pmatrix}\left[U_1^{N-n+1}(x,\xi)+U_2^{N-n}(x,\xi)\right]q^n(x)\\-\left[Q_1^{N-n+1}(x,\xi)+Q_2^{N-n}(x,\xi)\right]u^n(x)\end{pmatrix}\mathrm{d}\Gamma(x)+u^{\mathrm{ff}.N}(\xi) \tag{6}$$

In the above equation, $u^n(x)$ and $q^n(x)$ are displacement and traction on the boundary, respectively. $U_1^{N-n+1}+U_2^{N-n}$ and $Q_1^{N-n+1}+Q_2^{N-n}$ represent the time domain half-plane displacement and traction kernels, respectively, as Eqs. (7) and (8):

$$U_1^{N-n+1}+U_2^{N-n}=\frac{1}{2\pi}\left[\begin{pmatrix}(N-n+1)\cosh^{-1}\frac{(N-n+1)C\Delta t}{r}-\sqrt{(N-n+1)^2-(\frac{r}{C\Delta t})^2}\\-2(N-n)\cosh^{-1}\frac{(N-n)C\Delta t}{r}+2\sqrt{(N-n)^2-(\frac{r}{C\Delta t})^2}\\+(N-n-1)\cosh^{-1}\frac{(N-n-1)C\Delta t}{r}-\sqrt{(N-n-1)^2-(\frac{r}{C\Delta t})^2}\end{pmatrix}+\begin{pmatrix}(N-n+1)\cosh^{-1}\frac{(N-n+1)C\Delta t}{r'}-\sqrt{(N-n+1)^2-(\frac{r'}{C\Delta t})^2}\\-2(N-n)\cosh^{-1}\frac{(N-n)C\Delta t}{r'}+2\sqrt{(N-n)^2-(\frac{r'}{C\Delta t})^2}\\+(N-n-1)\cosh^{-1}\frac{(N-n-1)C\Delta t}{r'}-\sqrt{(N-n-1)^2-(\frac{r'}{C\Delta t})^2}\end{pmatrix}\right] \tag{7}$$

$$Q_1^{N-n+1}+Q_2^{N-n}=\frac{-1}{2\pi}\left[\begin{pmatrix}\frac{1}{r}\frac{\partial r}{\partial n}\left\{\begin{matrix}\sqrt{(N-n+1)^2-\left(\frac{r}{C\Delta t}\right)^2}-2\sqrt{(N-n)^2-\left(\frac{r}{C\Delta t}\right)^2}\\+\sqrt{(N-n-1)^2-\left(\frac{r}{C\Delta t}\right)^2}\end{matrix}\right\}\end{pmatrix}+\begin{pmatrix}\frac{1}{r'}\frac{\partial r'}{\partial n}\left\{\begin{matrix}\sqrt{(N-n+1)^2-\left(\frac{r'}{C\Delta t}\right)^2}-2\sqrt{(N-n)^2-\left(\frac{r'}{C\Delta t}\right)^2}\\+\sqrt{(N-n-1)^2-\left(\frac{r'}{C\Delta t}\right)^2}\end{matrix}\right\}\end{pmatrix}\right] \tag{8}$$

$u^{\mathrm{ff}.N}$ is also the free-field displacement of the smooth ground surface. In order to solve the spatial integral of Eq. (6), it must be discretized by a numerical scheme.

After meshing the boundaries using quadratic boundary elements, the following matrix-formed equation is obtained:

$$\sum_{n=1}^{N} \boldsymbol{H}^{N-n+1}\boldsymbol{u}^{n} = \sum_{n=1}^{N} \boldsymbol{G}^{N-n+1}\boldsymbol{q}^{n} + \boldsymbol{u}^{\mathrm{ff}.N} \tag{9}$$

where $\boldsymbol{H}^{N-n+1}$ and $\boldsymbol{G}^{N-n+1}$ are matrices whose components are determined by integrating on the boundary elements. $\boldsymbol{u}^{n}$ and $\boldsymbol{q}^{n}$ are the vectors of nodal values at time step n. $\boldsymbol{u}^{\mathrm{ff}.N}$ is a matrix consisting of the free-field displacement whose number of columns is equal to the number of time steps. In order to solve Eq. (9), the boundary conditions must be applied to the boundary nodes in a numerical approach. Equation (9) is rewritten as Eq. (10):

$$\boldsymbol{A}_{1}^{1}\boldsymbol{X}^{N} = \boldsymbol{B}_{1}^{1}\boldsymbol{Y}^{N} + \boldsymbol{R}^{N} + \boldsymbol{u}^{\mathrm{ff}.N} \tag{10}$$

where $\boldsymbol{X}^{N}$ and $\boldsymbol{Y}^{N}$ are vectors of unknown and known boundary values, respectively. $\boldsymbol{A}_{1}^{1}$ and $\boldsymbol{B}_{1}^{1}$ are matrices where the number of columns is equal to unknown and known boundary values and only needs to be calculated at the first time step. $\boldsymbol{R}^{N}$ shows the effect of dynamic time histories on the time node N and is expressed as follows:

$$\boldsymbol{R}^{N} = \sum_{n=1}^{N-1}\left(\boldsymbol{G}^{N-n+1}\boldsymbol{q}^{n} - \boldsymbol{H}^{N-n+1}\boldsymbol{u}^{n}\right) \tag{11}$$

All unknown boundary values, including displacement and traction fields, are determined by solving Eq. (10) at each step. The introduced method was successfully applied to concave topographies that lie below the smooth ground surface (Panji *et al*., 2013). To solve the topographies that are completely above the ground surface (convex topographies), a domain separation process was previously proposed and applied to homogeneous hill shaped features (Panji *et al*., 2014a). According to this process, non-homogeneous convex topography is divided into two domains as shown in Fig. 1. The first domain consists of a pitted half-plane as well as the interface with the hill as an open domain model, and the second domain, including the interface, plus the hill surface boundary as a closed domain model. The difference between the first and second sections is the absence of free-field motion in the equations of the second domain. After forming the discretized BIE for both domains, they are assembled to create a coupled equation. For this purpose, the conditions of continuity on the interface must be satisfied. These conditions are as follows:

$$u_{12}^{N} = u_{21}^{N} \tag{12}$$

$$\mu_1 q_{12}^{N} = -\mu_2 q_{21}^{N} \tag{13}$$

where μ_1 and μ_2 are the shear modulus of domains I and II, respectively. After applying the continuity condition at the interface, the assembled BIE is written in the following form:

$$\begin{bmatrix} H_{12}^{1} & H_{1}^{1} & 0 & -\dfrac{1}{\mu_1}G_{12}^{1} \\ H_{21}^{1} & 0 & H_{2}^{1} & \dfrac{1}{\mu_2}G_{21}^{1} \end{bmatrix} \begin{Bmatrix} u_{12}^{N} \\ u_{1}^{N} \\ u_{2}^{N} \\ q_{12}^{N} \end{Bmatrix} = \begin{bmatrix} G_{1}^{1} & 0 \\ 0 & G_{2}^{1} \end{bmatrix} \begin{Bmatrix} q_{1}^{N} \\ q_{2}^{N} \end{Bmatrix} + \begin{Bmatrix} R_{(1)}^{N} \\ R_{(2)}^{N} \end{Bmatrix} + \begin{Bmatrix} u_{(1)}^{\mathrm{ff}.N} \\ 0 \end{Bmatrix} \tag{14}$$

Considering that the governing boundary conditions on the seismic problems are always traction-free ($q_1^N = q_2^N = 0$), Eq. (14) is rewritten in the simplified form:

$$\begin{bmatrix} H_{12}^{1} & H_{1}^{1} & 0 & -\dfrac{1}{\mu_1}G_{12}^{1} \\ H_{21}^{1} & 0 & H_{2}^{1} & \dfrac{1}{\mu_2}G_{21}^{1} \end{bmatrix} \begin{Bmatrix} u_{12}^{N} \\ u_{1}^{N} \\ u_{2}^{N} \\ q_{12}^{N} \end{Bmatrix} = \begin{Bmatrix} R_{(1)}^{N} \\ R_{(2)}^{N} \end{Bmatrix} + \begin{Bmatrix} u_{(1)}^{\mathrm{ff}.N} \\ 0 \end{Bmatrix} \tag{15}$$

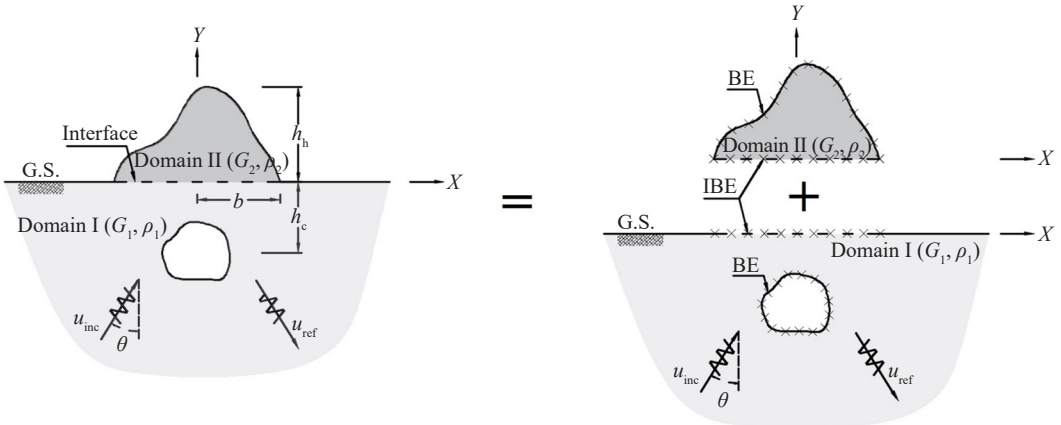

Fig. 1 Definition sketch for solving the alluvial hill problems using half-plane time domain BEM. IBE and BE indicate the interface and usual boundary elements, respectively

After solving Eq. (15) at each time step, all unknowns, such as displacement and traction fields on the interface, as well as the displacement of the hill surface and the boundary of cavity, are simply obtained. Also, to obtain the response at an internal point of m outside the topography on a smooth ground surface (u^m), the geometry coefficient of $c(\xi)$ in Eq. (3) is set equal to 1.0, so the equation can be rewritten as Eq. (16) for the internal points:

$$u^m(\xi,t)=\int_\Gamma \cdot \left\{\int_0^t\left[u^{*m}(x,t;\xi,\tau).q(x,\tau)-q^{*m}(x,t;\xi,\tau).u(x,\tau)\right]\mathrm{d}\tau\right\}\cdot \mathrm{d}\Gamma(x)+u^{\mathrm{ff}.m}(\xi,t) \tag{16}$$

The discretized form of Eq. (16) for domain I is written as follows:

$$\boldsymbol{u}^{N.m}=\sum_{n=1}^{N}\left(\begin{bmatrix}\frac{1}{\mu_1}G_{12}^{(N-n+1).m} & G_1^{(N-n+1).m}\end{bmatrix}\begin{Bmatrix}q_{12}^n\\ q_1^n\end{Bmatrix}\right)- \sum_{n=1}^{N}\left(\begin{bmatrix}H_{12}^{(N-n+1).m} & H_1^{(N-n+1).m}\end{bmatrix}\begin{Bmatrix}u_{12}^n\\ u_1^n\end{Bmatrix}\right)+\begin{Bmatrix}u_{12}^{\mathrm{ff}.N.m}\\ u_1^{\mathrm{ff}.N.m}\end{Bmatrix} \tag{17}$$

where $u^{N.m}$ is the displacement of the internal point m.

3 Validation examples

The above formulation was implemented in developing an algorithm previously named as DASBEM (Panji *et al*., 2013; Panji *et al*., 2014a, 2014b). In order to validate the method and the developed algorithm for analyzing alluvial convex topographies, three different hill models including a semi-circular hill, a semi-elliptical hill, and a Gaussian-shaped hill, located on an underground cavity were investigated by using the proposed method and the results were compared with the previous studies, all of which were without underground cavity. The results showed that by increasing the depth of the cavity (h_c), the effect of the cavity on the amplification of the hill surface was eliminated which is in good agreement with the previous studies and confirms the validity and effectiveness of the method. Since all of the previous studies were carried out in the homogeneous domain, the current examples are also studied for the homogeneous domain in order to make the comparison possible. The incident wave function used in this study is the Ricker wavelet (Ricker, 1953), which produces the free field displacement ($\boldsymbol{u}^{\mathrm{ff}}$) as follows:

$$\boldsymbol{u}^{\mathrm{ff}}(x,y,t)=a_{\max}\cdot\left(\left[1-2(\frac{\pi f_{\mathrm{p}}}{C}\alpha^{\mathrm{inc.}})^2\right]\mathrm{e}^{-(\frac{\pi f_{\mathrm{p}}}{C}\alpha^{\mathrm{inc.}})^2}H(t-\frac{r^{\mathrm{inc.}}}{C})+\left[1-2(\frac{\pi f_{\mathrm{p}}}{C}\alpha^{\mathrm{ref.}})^2\right]\mathrm{e}^{-(\frac{\pi f_{\mathrm{p}}}{C}\alpha^{\mathrm{ref.}})^2}H(t-\frac{r^{\mathrm{ref.}}}{C})\right) \tag{18}$$

in which:

$$\alpha^{\mathrm{inc.}}=C(t-t_0)+r^{\mathrm{inc.}};\quad r^{\mathrm{inc.}}=\left|-x\sin\theta+y\cos\theta\right| \tag{19}$$

$$\alpha^{\mathrm{ref.}}=C(t-t_0)+r^{\mathrm{ref.}};\quad r^{\mathrm{ref.}}=\left|-x\sin\theta-y\cos\theta\right| \tag{20}$$

where $a_{\max}$,f_{p}, t_0 and H are the maximum displacement of the time history, the predominant frequency, the time shift parameter and the Heaviside step function, respectively. The dimensionless frequency (η) is obtained from the following equation:

$$\eta=\frac{\omega b}{\pi C} \tag{21}$$

where ω is the angular frequency of the wave, b is the half-width of the hill, and C is the shear wave velocity. As can be seen in Fig. (1), study parameters include the half-width of the hill (b), the height of the hill (h_{h}), the radius of the cavity (a) and the cavity depth (h_{c}) as geometry parameters; the shear modulus (μ) and the density (ρ) of the domain as material parameters; the dimensionless frequency (η) and wave angle (θ) as wave parameters; the parameters of Ricker wavelet including f_{p} and t_0 and the maximum displacement ($a_{\max}$) and the time step of discretization (Δt) as parameters of the numerical solution. The corresponding values of these parameters for validation study cases are shown in Table 1.

In the first example, a semi-circular hill located on an underground cavity was studied using this method. To investigate the effect of changes of time step and nodes interval at the stability of time domain BEM analysis and select the proper values, the dimensionless parameter β defined as:

$$\beta=\frac{\Delta t\cdot C}{\Delta l} \tag{22}$$

where C, Δt and Δl are shear wave velocity, time step and distance between nodes, respectively. In fact, parameter β indicates the number of elements in a time step when the seismic wave passes. In the use of time steps, it is recommended that β be close to 1 for elastodynamics problems with uniform meshes (Dominguez & Gallego, 1991). Thus, the effect of parameter β is investigated for this example with the assumed data in Table 1. The shear wave velocity was equal to 900 m/s; the values of time steps were equal to five values of 0.0034, 0.013, 0.022, 0.034 and 0.044 s. and the distance of the nodes was equal to 10 m for the first time step value and 20 m for others (i.e., considering 31 nodes, only on the surface of the hill). This change caused β to be 0.3 to 2.0, respectively. In Fig. 2, the time domain ground response for top points

Table 1 Parameter values of the validation study cases: 1. Semi-circular hill; 2. Semi-elliptical hill; 3. Gaussian-shaped hill

Case	b (m)	h_h	a	h_c	μ (MPa)	ρ (t/m^3)	η	θ ($^\circ$)	f_p (Hz)	t_0 (s)*	a_{max} (m)	Δt (s)	Δl (m)
1	200	b	0.4b	b – 20b	1440	1.8	1	0 & 30	2	2 – 5	0.001	0.022	20
2(a)	300	2/3b	0.4b	b – 10b	1440	1.8	2	0 & 90	3	2 – 7	0.001	0.020	20
2(b)	300	2b	0.4b	b – 15b	6525	2.9	0.5 &1	0	3	2–7	0.001	0.020	20
3	200	0.5b	0.4b	b – 10b	1440	1.8	0.5	0 & 90	3	1.5 – 5.5	0.001	0.020	20

* t_0 value differs between two given values depending on h_c

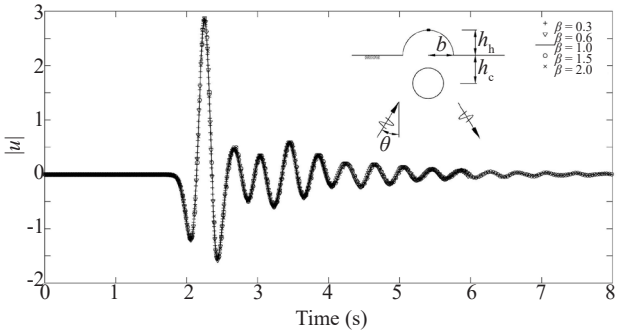

Fig. 2 Time domain displacement at the top point of semi-circular hill for different values of β

of the hill surface is given. As can be seen, the responses were steady with the change of the β parameter. Hence, to optimize the number of time steps and obtain an acceptable response, β was chosen as 1 in this study.

The results obtained from solving this example were compared with the analytical solutions of Yuan and Men (1992) and Tsaur and Chang (2009) on the hill without a cavity. The result showed that by increasing the depth of the cavity (h_c) to about 15-20 times the hill half-width (b), the effect of the cavity on the amplification of the hill surface was eliminated and the results coincided with the previous studies (Fig. 3).

For the second verification, a semi-elliptical hill located on an underground circular cavity in two cases of a shallow and deep hill, was modeled by this method. The corresponding values of the parameters are shown in Table 1 (cases 2(a) and 2(b), respectively). The results were compared with the previous studies by Chen *et al*. (2012) and Liang and Fu (2011) for each case, respectively. Chen *et al*. (2012) presented a semi-analytical approach for analyzing the seismic semi-elliptical shallow hills and Liang and Fu (2011) used a closed-form analytical solution for its deep case. The results of the comparison shown in Figs. 4 and 5 for cases 2(a) (shallow hill) and 2(b) (deep hill), respectively, confirm the correct operation of the method and algorithm used.

For the third example, a Gaussian-shaped hill, according to Eq. (23), on an underground circular cavity was studied. The parameter values for this case are shown in Table 1 (case 3). The results were compared by full-plane BEM solutions of Sanchez-Sesma *et al*. (1982). As can be seen in Fig. 6, the comparison results are in a good agreement.

$$y = h_h\left(1-\left(x/b\right)^2\right)\mathrm{e}^{-3\left(\frac{x}{b}\right)^2} \tag{23}$$

4 Numerical study

For numerical study, according to Eq. (24) a semi-sine shaped alluvial hill located on an underground circular cavity (Fig. 7) was studied subjected to propagating incident SH-waves. The hill shape ratio ($S_r = h_h / b$) considered as 2, 1, 0.75 and 0.50, and the cavity depth ratio ($h_r = h_c / b$) was equal to 2.50. The Ricker wavelets with predominate frequency of f_p = 3 Hz was applied to the model in two incident angles: vertical and horizontal.

$$\begin{cases} y = 0.5h_h\left(1+\cos\left(\dfrac{\pi x}{b}\right)\right), & |x| < b \\ y = 0, & |x| \geq b \end{cases} \tag{24}$$

Shear wave velocity in each domain and the impedance ratio are as follows:

$$C_i = \sqrt{\frac{\mu_i}{\rho_i}};\ i = 1,2 \tag{25}$$

$$I = \frac{\rho_2 \cdot C_2}{\rho_1 \cdot C_1} \tag{26}$$

For parametric studies, three different cases were considered (Geli *et al*., 1988). The density values (ρ), shear wave velocity (C) and impedance ratios (I) in the cases are listed in Table 2. Index 1 and 2 are for an underlying half-space and a hill domain, respectively. Case a is a homogeneous hill, case b models a hill with more soft materials than

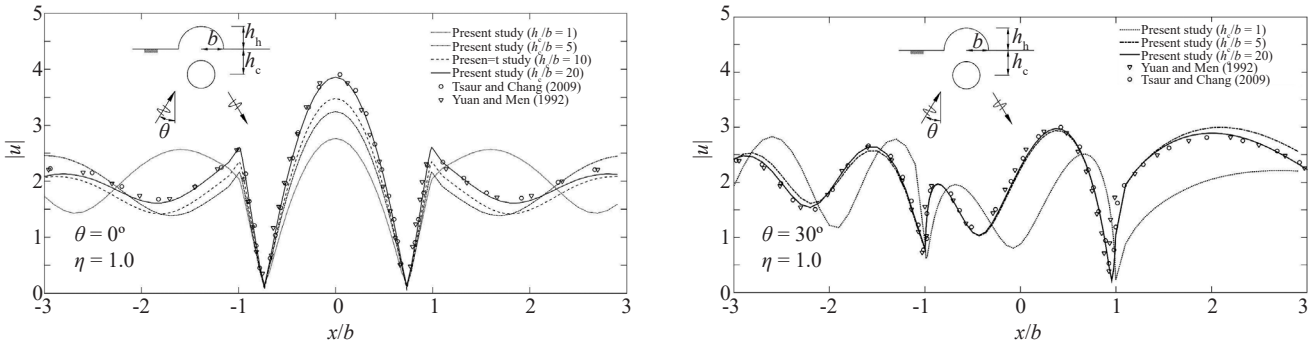

Fig. 3 Normalized displacement amplitudes of uniform semi-circular hill surface above subsurface circular cavity at dimensionless frequency of 1.0 subjected to SH-wave with angles: 0º and 30º

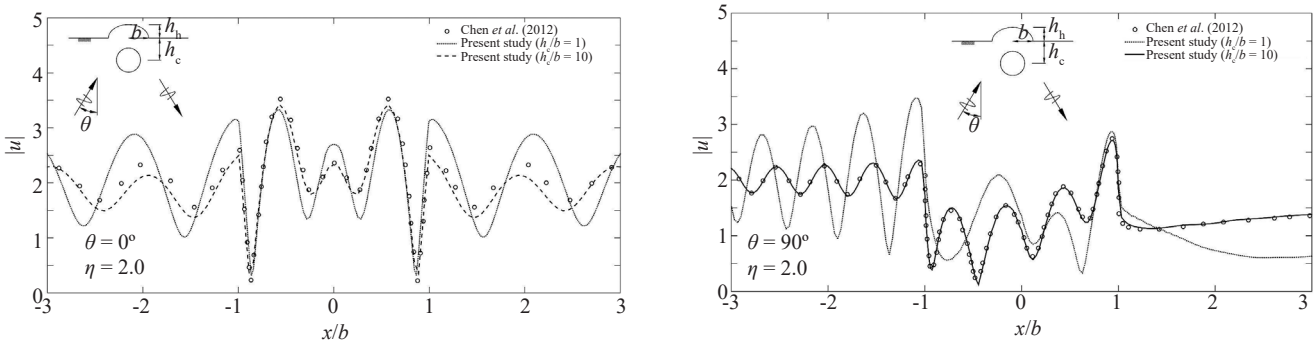

Fig. 4 Normalized displacement amplitudes of shallow semi-elliptical hill surface above subsurface circular cavity at dimensionless frequency of 2.0 subjected to SH-wave with angles: 0º and 90º

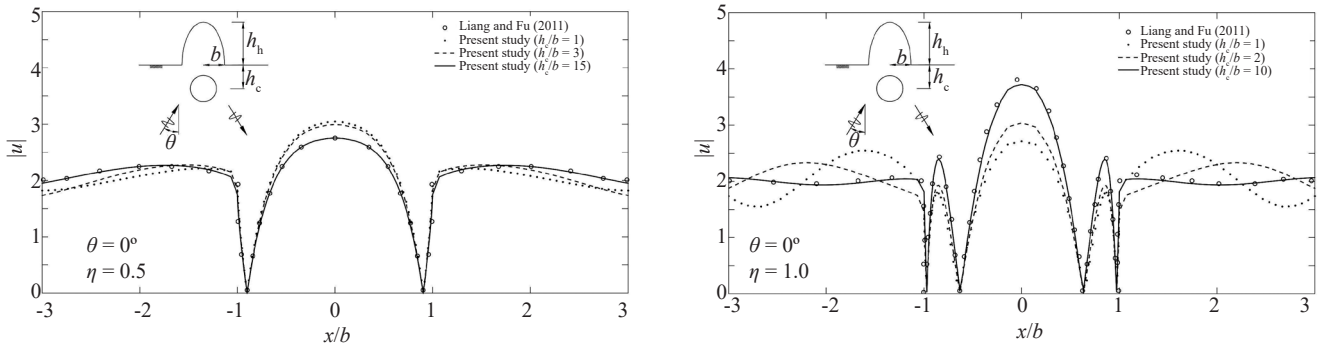

Fig. 5 Normalized displacement amplitudes of deep semi-elliptical hill surface above subsurface circular cavity at dimensionless frequency of 0.5 and 1.0 subjected to vertical SH-wave

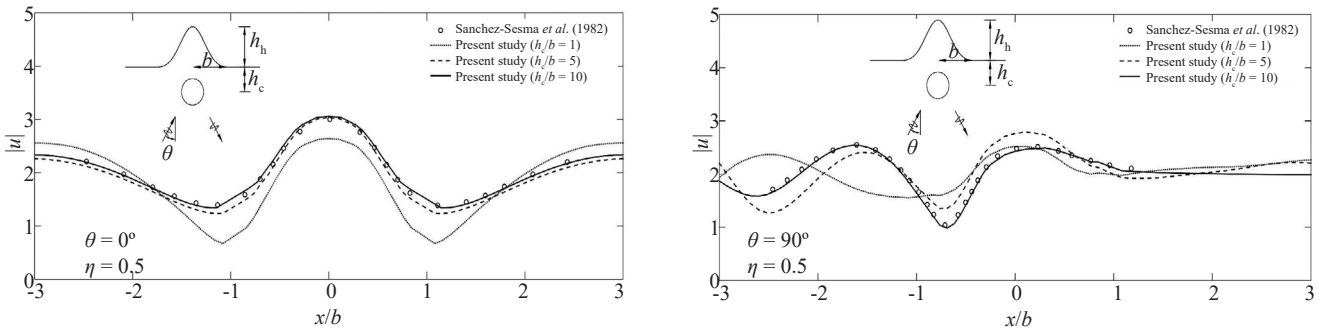

Fig. 6 Normalized displacement amplitudes of uniform Gaussian-shaped hill surface above subsurface circular cavity at dimensionless frequency of 0.5 subjected to SH-wave with angles: 0º and 90º

the underlying environment; for example, a hill of Tuff material (soft igneous sedimentary rock) with a density of 1.92 t/m^3 and shear wave velocity of 700 m/s located on a half-space of Conglomerate (firm rock) with density of 2 t/m^3 and shear wave velocity of 840 m/s. Case c is a hill with harder materials than the underlying environment; for example, a hill of dense gravely soil with a density of 1.98 t/m^3 and shear wave velocity of 440 m/s located on a half-space of stiff clay with density of 1.90 t/m^3 and shear wave velocity of 350 m/s. Other parameters are assumed as in previous examples. The effect of different factors on the response of the hill surface was studied separately and the results are discussed below. First, the effect of the impedance ratio and then the effect of the shape ratio of the hill were investigated on the amplification factor of the ground surface response.

4.1 Effect of impedance ratio

According to Table 2, three values of 1, 0.80, and 1.30 are considered for the impedance coefficients as homogenous, soft and hard hills, respectively. In this regard, the shape ratio of the hill is assumed equal to 1.0 (S_r = 1.0). The wave incident angle is considered as vertical and horizontal cases and the results are evaluated in the two domains of time and frequency.

4.1.1 Synthetic seismograms

Figures 8 and 9 show the time domain response of the hill surface subjected to incident SH-waves in two cases of vertical and horizontal, respectively. The results display that increasing the hill impedance coefficient relative to the underlying domain leads to a decrease in the magnitude of the riser hill response (x/b=0) but it does not affect the response at the corner of the hill (x/b=1). Meanwhile, with the decrease of the impedance coefficients, the wave's diffraction on the hill range is increased and rapidly depreciated. It is clear that as the hill becomes softer than the underlying domain, the surface response includes critical states and, subsequently the structures located on the ground are faced with more risk against earthquake loads. Although the wave's diffraction on the hill is great in the horizontal incident waves, the amplitudes are significantly reduced, especially in the case of the soft hill. As can be seen in these figures, the trapped waves obtained after direct/reflected waves take perfectly the shape of the hill and repeated regularly until convergence. In the case of hard hill, this repetition process is clearly visible for vertical incident waves. Nevertheless, for horizontal waves, the trapped wave's repetition is obviously illustrated in the case of homogeneous hill.

Table 2 Considered parameters for different cases

Case	ρ_1/ρ_2	C_1/C_2	I
a (homogeneous hill)	1.0	1.0	1.0
b (soft hill)	1.04	1.2	0.8
c (hard hill)	0.96	0.8	1.3

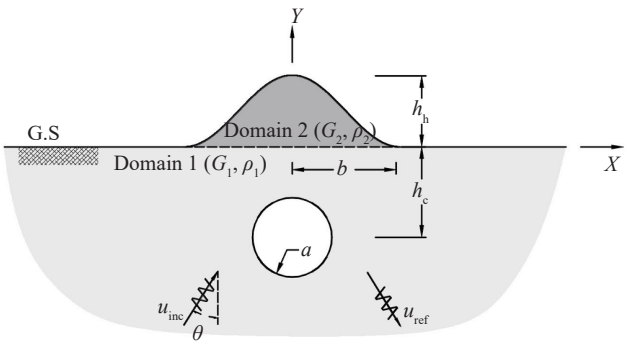

Fig. 7 Schematic model for an alluvial semi-sine shaped hill above an underground circular cavity subjected to propagating obliquely incident SH-waves

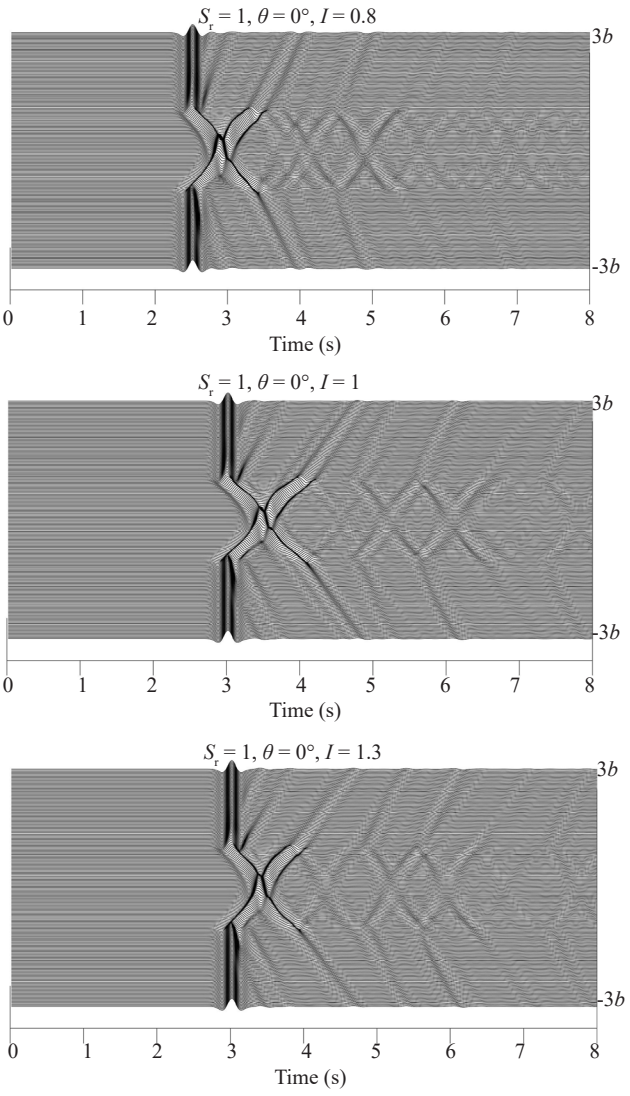

Fig. 8 Synthetic seismograms of the surface of semi-sine shaped hill above subsurface circular cavity subjected to vertical incident SH-waves including shape ratio of 1.0 and impedance factors 0.8, 1.0 and 1.3

4.1.2 Amplification pattern

In Figs. 10 and 11, the results of the frequency domain investigations are presented for the two angle of wave incident in different impedance ratios. In these figures, the amplification factor of the surface is illustrated versus dimensionless frequency (η). This factor is defined as the ratio of the surface response to free-field motion. As can be seen in Fig. (10), by increasing the impedance ratio or in the other words with hardening the hill, the amplification of the surface is approximately reduced with a fixed trend. In the case of the soft hill, the maximum amplification occurred close to the dimensionless frequency of 1.5. However, in the case of the hard hill, an extreme value is illustrated between 1 and 1.5. The pattern of response fluctuations is always the same in all figures. A noteworthy point is that in small dimensionless frequencies (less than 1), the amplification peak is placed on the top of the

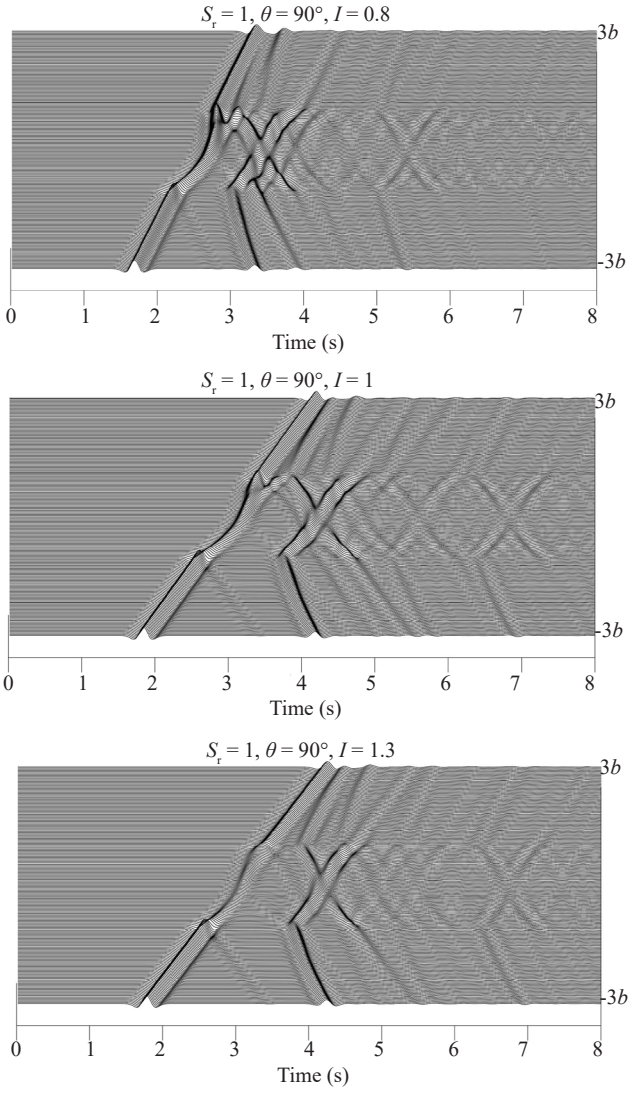

Fig. 9 Synthetic seismograms of the surface of semi-sine shaped hill above subsurface circular cavity subjected to horizontal incident SH-waves including shape ratio of 1.0 and impedance factors 0.8, 1.0 and 1.3

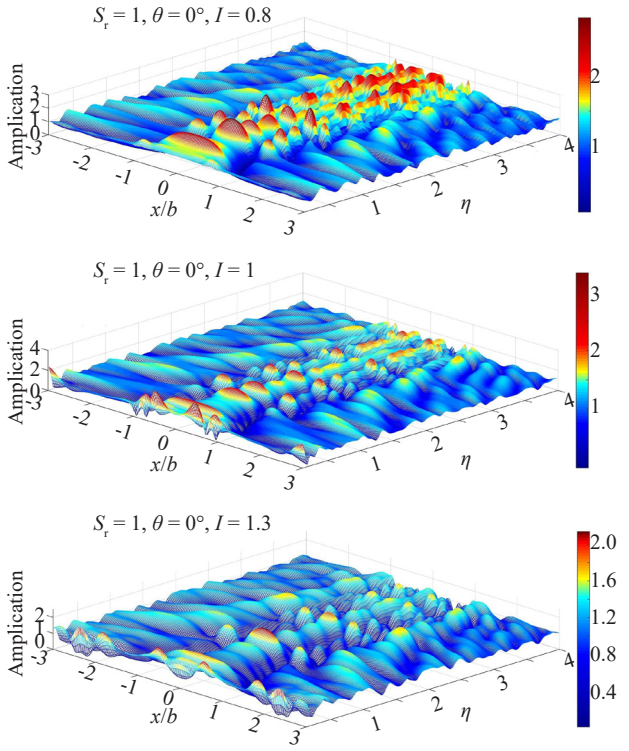

Fig. 10 Amplification patterns of the surface of semi-sine shaped hill above subsurface circular cavity subjected to vertical incident SH-waves including shape ratio of 1.0 and impedance factors 0.8, 1.0 and 1.3

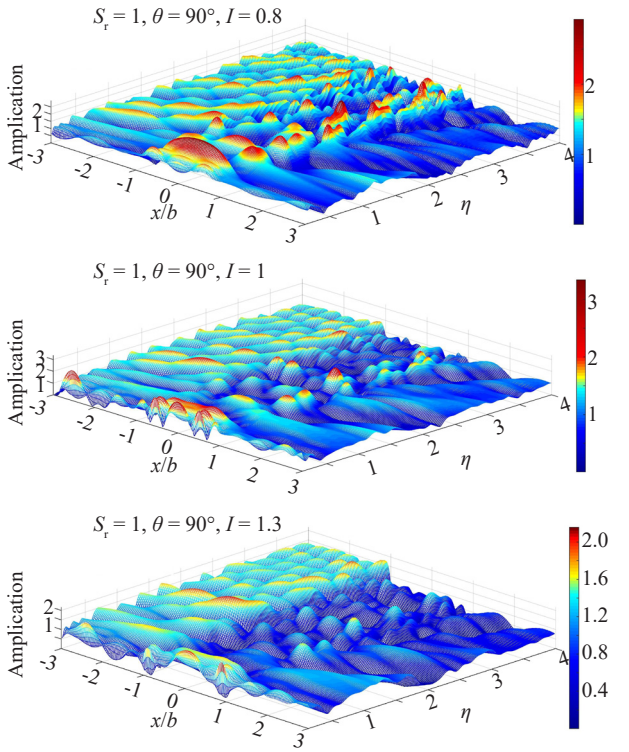

Fig. 11 Amplification patterns of the surface of semi-sine shaped hill above subsurface circular cavity subjected to horizontal incident SH-waves including shape ratio of 1.0 and impedance factors 0.8, 1.0 and 1.3

hill, while it is moved to the corners of the hill when the dimensionless frequency increases and with more increase in the frequency, the peak moves back toward the hill side.

The effect of the existence of the cavity on the responses is illustrated in the case of horizontal incident waves (Fig. 11). As can be seen, the fluctuations obtained on the responses are de-amplified behind the wave front on the smooth ground surface, i.e., in the range of 1*b* to 3*b*. In this case, the amplification is also reduced on the hill surface by increasing the impedance ratio, so that the minimum values are observed in the case of the hard hill (I=1.3). In this case, note that the amplification is only focused on the smooth ground near the wave front. Furthermore, increasing the impedance ratio has a negative effect on the oscillation of the responses because the most swing of the ground surface is experienced in the case of the soft hill.

4.2 Effect of shape ratio

To investigate the effect of the shape ratio (the ratio of the height to half-width of the hill) on the surface response, the values of 2, 1, 0.75 and 0.5 were considered. In this study, the impedance and depth ratios ($h_r = h_c / b$) were assumed as 0.8 and 2.5, respectively. As in previous sections, the incident SH-wave is applied to the model with two vertical and horizontal angles. The results are depicted in Figs. 12 to 15 for the time and frequency domains. According to the synthetic seismograms of vertical incident waves (Fig. 12), by decreasing the shape ratio, the amplitude of the response on the hill (x/b=0) is reduced. As can be seen, the form of the hill appears on the surface as well, so that the hill with a shape ratio of 2.0 has the most circular form of the trapped waves and this circle is always compressed by shrinking the hill size. This behavior is similarly observed in the horizontal incident waves (Fig. 13), with the difference that the wave's diffraction is realized with more clarity in this case.

To show the effect of the hill size on the amplitude of the responses, the amplification patterns are presented in Figs. 14 and 15. Increasing the shape ratio has a positive effect on the responses, especially above the hill. As can be seen, the shape ratio of 2.0 shows a critical state for the patterns in the case of vertical incident, because the rate of amplification is about 3.5 on the hill. In the low frequencies (less than 1.5), the middle of the hill includes the maximum amplification, but the edges are substituted by increasing the frequency. By decreasing the shape ratio, the same situation is almost formed, namely the amplification of the hill crest disappears. Although the number of fluctuations on the sides of the hill are reduced by its shrinking, the height of the created peaks/valleys are deeply formed. In the case of horizontal incident waves (Fig. 15), the amplification is approximately observed close to the wave front with high oscillations. By increasing the frequency, the peaks are moved from the center of hill towards its corners. Note that the critical state on the responses occurred at the corner that is farther away from the wave front. As can be seen in all figures, the role of seismic isolation of the cavity is always observed behind the incoming wave front on the ground surface.

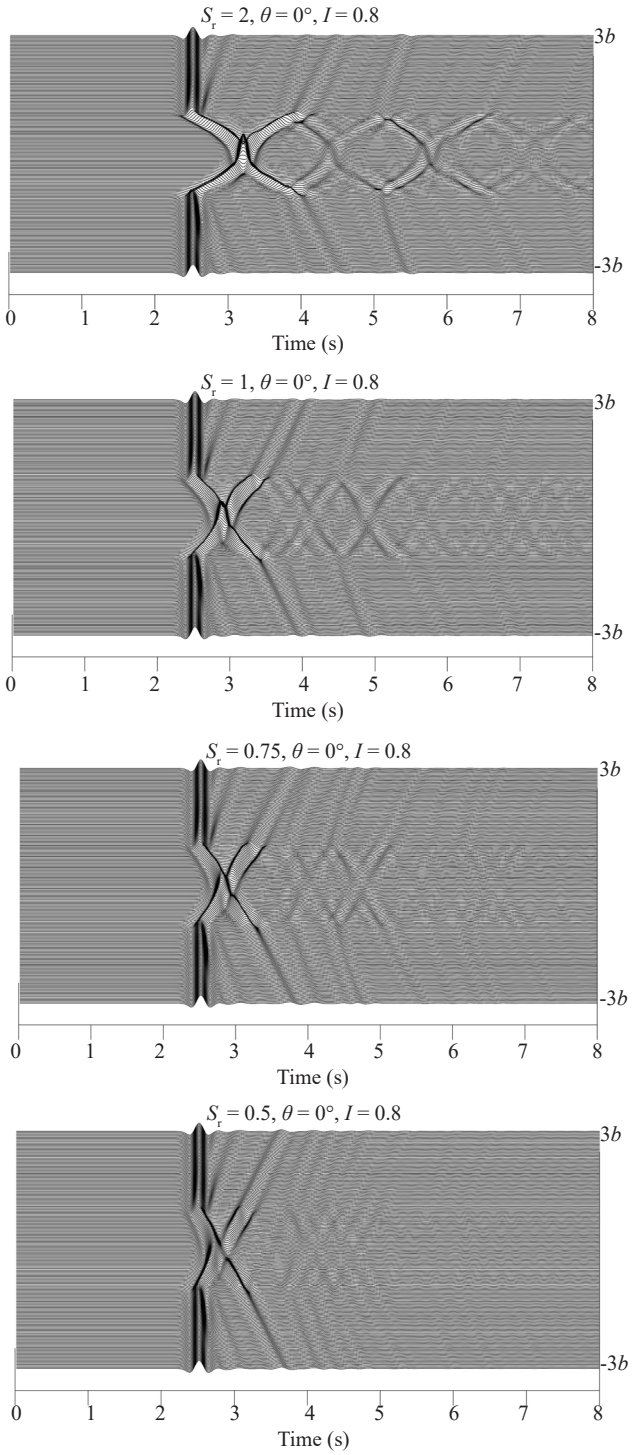

Fig. 12 Synthetic seismograms of the surface of semi-sine shaped hill above subsurface circular cavity subjected to vertical incident SH-waves including impedance factor of 0.8 and shape ratios 2.0, 1.0, 0.75 and 0.5

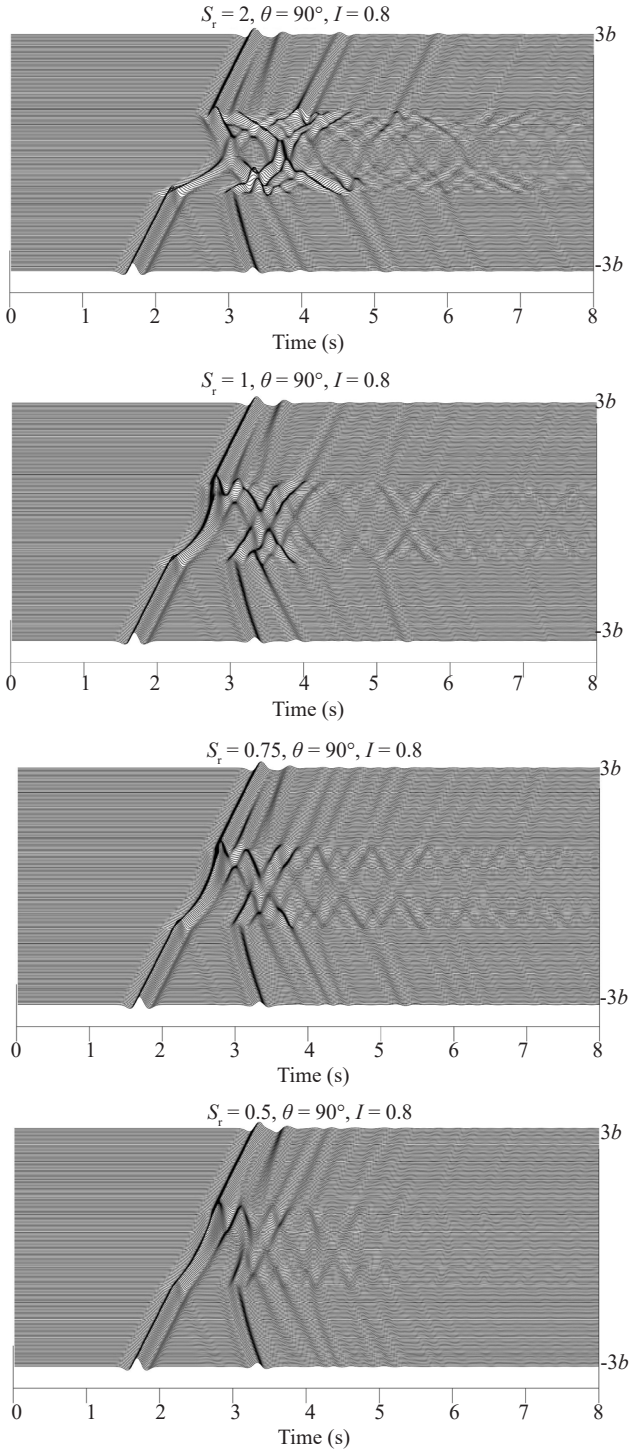

Fig. 13 Synthetic seismograms of the surface of semi-sine shaped hill above subsurface circular cavity subjected to horizontal incident SH-waves including impedance factor of 0.8 and shape ratios 2.0, 1.0, 0.75 and 0.5

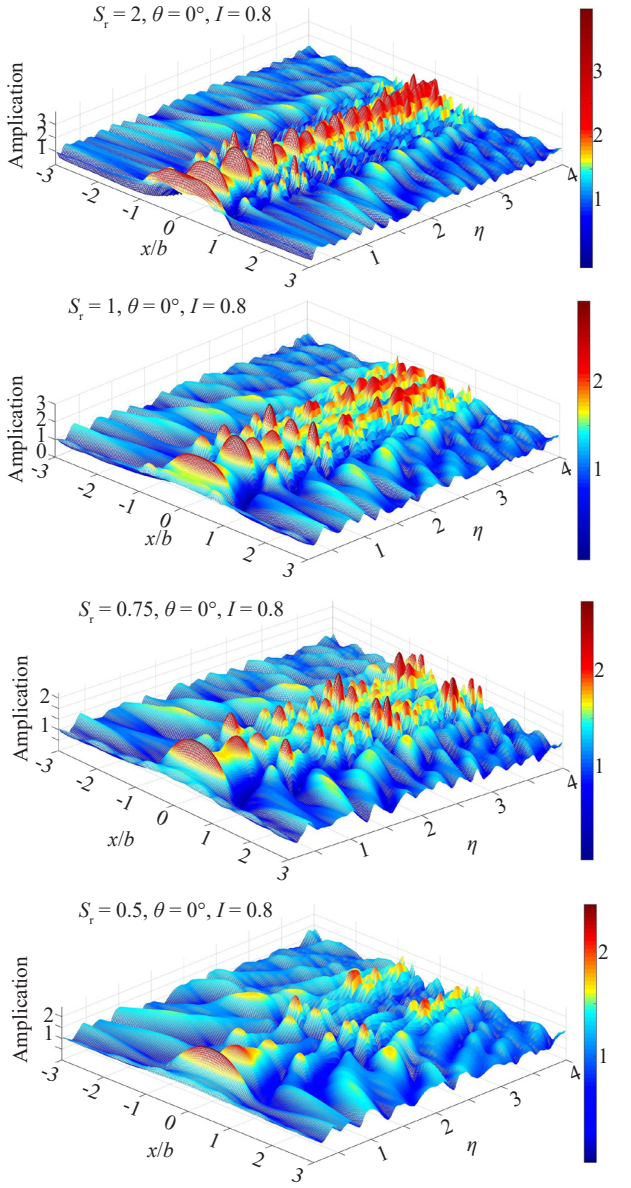

Fig. 14 Amplification patterns of the surface of semi-sine shaped hill above subsurface circular cavity subjected to vertical incident SH-waves including impedance factor of 0.8 and shape ratios 2.0, 1.0, 0.75 and 0.5

5 Conclusions

A half-plane time domain BEM was applied to present the seismic response of a semi-sine shaped alluvial hill above a subsurface circular cavity, subjected to propagating incident SH-waves. After solving some verification examples, it was seen that the method was able to analyze the combined heterogeneous topographic problems. Then, by considering two intended parameters including impedance and hill shape ratios, a sensitivity analysis was successfully carried out to obtain the surface response under vertically/horizontally incident SH-waves. The models were elaborated in three impedance ratios of 0.8, 1.0 and 1.3 as soft, uniform and hard hill, respectively. Also, four shape ratios were considered for the size of hills as 0.5, 0.75, 1.0 and 2.0. The depth of the cavity was fixed in all the analyses. The results are presented as synthetic seismograms and amplification patterns. The results of the parametric study can be

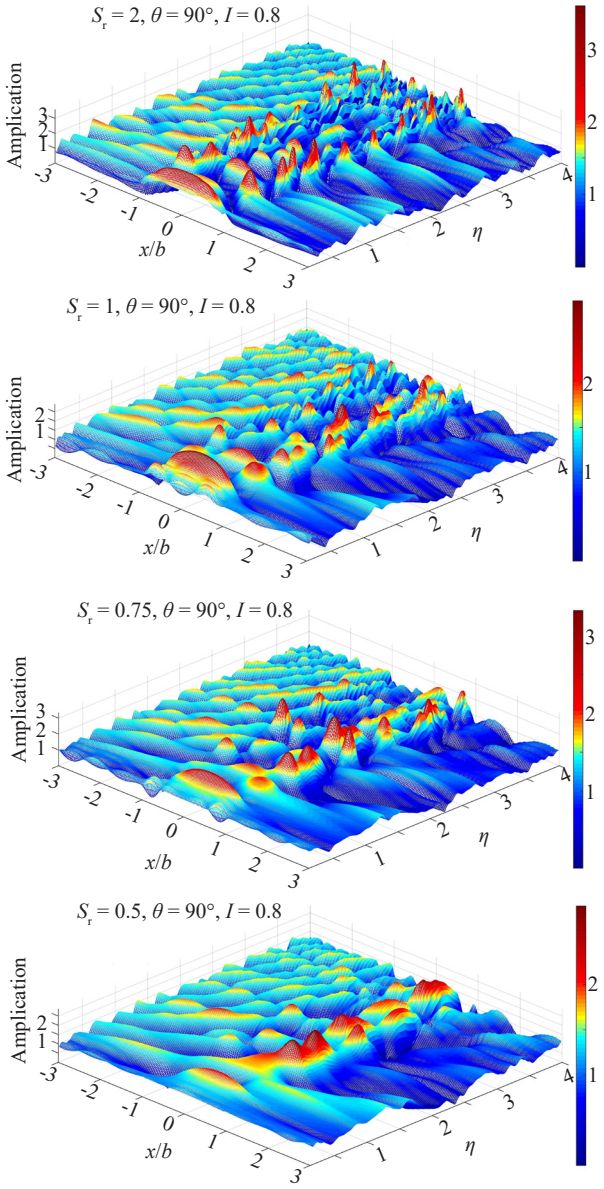

Fig. 15 Amplification patterns of the surface of semi-sine shaped hill above subsurface circular cavity subjected to horizontal incident SH-waves including impedance factor of 0.8 and shape ratios 2.0, 1.0, 0.75 and 0.5

summarized as follows:

1. The surface response was absolutely influenced by the dimensions/material properties of the hill.
2. The synthetic seismograms of the surface showed that obtaining the trapped waves after the reflected waves seemed like a closed circular zone, where the impedance ratio was effective on its amplitudes. Also, these zones were proportional to the size of the hill.
3. Amplification patterns showed that the maximum amplitudes were significantly reduced by hardening the hill about 40%.
4. The seismic isolation role of the existence of the cavity was observed on the surface response located beyond the hill behind the incoming wave front.
5. By hardening the hill, the amplification was only focused on the smooth surface close to the arriving wave front in the case of horizontal incident waves.
6. Amplification patterns of the shape ratio effect showed that, in the case of vertical incident waves, the maximum value appeared on the hill center at low frequencies, and moved towards the corners by increasing the frequency. Moreover, in the case horizontal waves, the corner away from the wave front had a critical response when the hill size became smaller.

References

Aki K and Larner KL (1970), "Surface Motion of a Layered Medium Having an Irregular Interface due to Incident Plane SH Waves," *Journal of Geophysical Research*, **75**(5): 933–954.

Amornwongpaibun A and Lee VW (2013), "Scattering of Anti-Plane (SH) Waves by a Semi-Elliptical Hill: II—Deep Hill," *Soil Dynamics and Earthquake Engineering*, **52**: 126–137.

Amornwongpaibun A, Luo H and Lee VW (2015), "Scattering of Anti-Plane (SH) Waves by a Shallow Semi-Elliptical Hill with a Concentric Elliptical Tunnel," *Journal of Earthquake Engineering*, **20**(3): 363–382.

Ausilio E, Conte E and Dente G (2008), "Seismic Response of Alluvial Valleys to SH Waves," *Seismic Engineering Conference, AIP Conference Proceedings*, **1020**: 199–206.

Ba Z, Liang J and Zhang Y (2016), "Scattering and Diffraction of Plane SH-Waves by Periodically Distributed Canyons," *Earthquake Engineering and Engineering Vibration*, **15**(2): 325–339

Ba Z, Liang J and Zhang Y (2017), "Diffraction of SH-Waves by Topographic Features in a Layered Transversely Isotropic Half-Space," *Earthquake Engineering and Engineering Vibration*, **16**(1): 11–22.

Bard PY (1982), "Diffracted Waves and Displacement Field over Two-Dimensional Elevated Topographies," *Geophysical Journal International*, 71(3): 731–760.

Belytschko T and Chang HS (1988), "Simplified Direct Time Integration Boundary-Element Method," *Journal of Engineering Mechanics*, **114**(1): 117–134.

Boor DM (1972), "A Note on the Effect of Simple Topography on Seismic SH Waves," *Bulletin of the Seismological Society of America*, **62**(1): 275–284.

Boor DM (1973), "The Effect of Simple Topography on Seismic Waves: Implications for the Accelerations Recorded at Pacoima Dam, San Fernando Valley, California," *Bulletin of the Seismological Society of America*, **63**(5): 1603–1609.

Bouchon M (1973), "Effect of Topography on Surface Motion," *Bulletin of the Seismological Society of America*, **63**(3): 615–632.

Brebbia CA and Dominguez J (1989), *Boundary Elements, an Introductory Course*, Comp Mech Pub. Southampton, Boston.

Cao XR, Song TS and Liu DK (2001), "Scattering of Plane SH-Wave by a Cylindrical Hill of Arbitrary Shape," *Applied Mathematics and Mechanics*, **22**(9): 1082–1089.

Chen JT, Lee JW and Shyu WS (2012), "SH-Wave Scattering by a Semi-Elliptical Hill Using a Null-Field Boundary Integral Equation Method and a Hybrid Method," *Geophysical Journal International*, **188**: 177–194.

Chen JT, Lee JW, Wu ChF and Chen IL (2011), "SH-Wave Diffraction by a Semi-Circular Hill Revisited: A Null-Field Boundary Integral Equation Method Using Degenerate Kernels," *Soil Dynamics and Earthquake Engineering*, **31**(5-6): 729–736.

Datta SK (1974), "Diffraction of SH-Waves by an Elliptic Elastic Cylinder," *International Journal of Solids Structures*, **10**(1): 123–133.

Datta SK and Shah AH (1982), "Scattering of SH Waves by Embedded Cavities," *Wave Motion*, **4**(3): 265–283.

Day SM (1977), "Finite Element Analysis of Seismic Scattering Problems," *PhD Thesis*, University Of California, San Diego.

Ding G and Dravinski M (1996), "Scattering of SH Waves in Multilayered Media with Irregular Interfaces," *Earthquake Engineering and Structural Dynamics*, **25**: 1391–1404.

Dominguez J (1993), *Boundary Elements in Dynamics*, Comp Mech Pub, Southampton, Boston.

Dominguez J and Gallego R (1991), "The Time Domain Boundary Element Method for Elastodynamic Problems," *Math. Comput. Modelling*, **15**(3-5): 119–129.

Dominguez J and Meise T (1991), "On the Use of the BEM for Wave Propagation in Infinite Domains," *Engineering Analysis with Boundary Elements*, **8**(3): 132–138.

Dravinski M (1980), "Scattering of Elastic Waves by an Alluvial Valley of Arbitrary Shape," *Report No. CE 80-06*, *Department of Civil Engineering*, University of Southern California, Los Angeles, California.

Geli L, Bard PY and Jullien B (1988), "The Effect of Topography on Earthquake Ground Motion: a Review and New Results," *Bulletin of the Seismological Society of America*, **78**(1): 42–63.

Hadley PK (1987), "Scattering of Waves by Inclusions in a Nonhomogeneous Elastic Half Space Solved by Boundary Element Method," *PhD Thesis*, Princeton University, Princeton, United States.

Heather PB. and Lee VW (2017), "Scattering and Diffraction of Plane P-Waves in a 2-D Eastic Half-Space II: Shallow Arbitrary Shaped Canyon," *Earthquake Engineering and Engineering Vibration*, **16**(3): 459–485.

Kamalian M, Gatmiri B and Sohrabi-Bidar A (2003), "On Time domain Two-Dimensional Site Response Analysis of Topographic Structures by BEM," *Journal of Seismology and Earthquake Engineering*, Tehran, **5**(2): 35–45.

Kamalian M, Jafari MK, Sohrabi-Bidar A and Razmkhah A (2008), "Seismic Response of 2-D Semi-Sine Shaped Hills to Vertically Propagating Incident Waves: Amplification Patterns and Engineering Applications," *Earthquake Spectra*, **24**(2): 405–430.

Kamalian M, Jafari MK, Sohrabi-Bidar A, Razmkhah A and Gatmiri B (2006), "Time Domain Two-Dimensional Site Response Analysis of Non-Homogeneous Topographic Structures by a Hybrid BE/FE Method," *Soil Dynamics and Earthquake Engineering*, **26**: 753–765.

Lee VW (1988), "Three-Dimensional Diffraction of Elastic Waves by a Spherical Cavity in an Elastic Half-Space, I: Closed-Form Solutions," *Soil Dynamics and Earthquake Engineering*, **7**(3): 149–161.

Lee VW and Amornwongpaibun A (2013), "Scattering of Anti-Plane (SH) Waves by a Semi-Elliptical Hill: I - Shallow Hill," *Soil Dynamics and Earthquake Engineering*, **52**: 116–125.

Lee VW, Luo H and Liang J (2004), "Diffraction of Anti-Plane SH Waves by a Semi-Circular Cylindrical Hill with an Inside Concentric Semi-Circular Tunnel," *Earthquake Engineering and Engineering Vibration*, **3**(2): 249–262.

Lee VW, Luo H and Liang JW (2006), "Antiplane (SH) Wave Diffraction by a Semicircular Cylindrical Hill Revisited: An Improved Analytic Wave Series Solution," *Journal of Engineering Mechanics*, **132**(10): 1106–1114.

Liang J, Zhang Y and Lee VW (2005), "Scattering of Plane P Waves by a Semi-Cylindrical Hill: Analytical Solution," *Earthquake Engineering and Engineering Vibration*, **4**(1): 28–36.

Liang JW, Luo H and Lee VW (2004), "Scattering of Plane SH Waves by a Circular-Arc Hill with a Circular Tunnel," *Acta Seismologica Sinica*, **17**(5): 549–563.

Liang JW, Luo H and Lee VW (2010), "Diffraction of Plane SH Waves by a Semi-Circular Cavity in Half-Space," *Earthquake Science*, **23**(1): 5–12.

Liang J and Fu J (2011), "Surface Motion of a Semi-Elliptical Hill for Incident Plane SH Waves," *Earthquake Science*, **24**: 447–462.

Lin S, Qiu F and Liu D (2010), "Scattering of SH Waves by a Scalene Triangular Hill," *Earthquake Engineering and Engineering Vibration*, **9**(1): 23–38.

Lin H and Liu D (2002), "Scattering of SH-Wave Around a Circular Cavity in a Half Space," *Earthquake Engineering and Engineering Vibration*, **2**(2): 9–16.

Liu G, Chen H, Liu D and Khoo BC (2010), "Surface Motion of a Half-Space with Triangular and Semicircular Hills under Incident SH Waves," *Bulletin of the*

Seismological Society of America, **100**(3): 1306–1319.

Liu Q, Wu Z and Lee VW (2019), "Scattering and Reflection of SH Waves Around a Slope on an Elastic Wedged Space," *Earthquake Engineering and Engineering Vibration*, **18**(2): 255–266.

Luo C, Lou M, Gui G and Wang H (2019), "A Modified Domain Reduction Method for Numerical Simulation of Wave Propagation in Localized Regions," *Earthquake Engineering and Engineering Vibration*, **18**(1): 35–52.

Luo H, Lee VW and Liang J (2010), " Anti-Plane (SH) Waves Diffraction by an Underground Semi-Circular Cavity: Analytical Solution," *Earthquake Engineering and Engineering Vibration*, **9**(3): 385–396.

Lu X and Liu D (2006), "Ground Motion of a Semi-Cylindrical Hill and a Semi-Cylindrical Canyon Caused by Incident SH Wave," *Earthquake Engineering and Engineering Vibration*, **26**(5): 14–20.

Moczo P (1989), "Finite-Difference Technique for SH-Waves in 2-D Media Using Irregular Grids-Application to the Seismic Response Problem," *Geophysical Journal International*, **99**(2): 321–329.

Moeen-Vaziri N and Trifunac MD (1988), "Scattering and Diffraction of Plane SH-Waves by Two-Dimensional Inhomogeneities: Part I," *Soil Dyn. Earthq. Eng*., **7**(4): 179–188.

Mogi H and Kawakami H (2007), "Analysis of Scattered Waves on Ground with Irregular Topography Using the Direct Boundary Element Method and Neumann Series Expansion," *Bulletin of the Seismological Society of America*, **97**(4): 1144–1157.

Nowak SP and Hall JF (1993), "Direct Boundary Element Method for Dynamics in a Half-Space," *Bull. Seism. Soc. Am*., **83**(5): 1373-1390.

Ohtsu M and Uesugi S (1985), "Analysis of SH Wave Scattering in a Half Space and Its Applications to Seismic Responses of Geological Structures," *Eng. Anal*., **2**(4): 198–204.

Panji M and Ansari B (2017a), "Modeling Pressure Pipe Embedded in Two-Layer Soil by a Half-Plane BEM," *Computers and Geotechnics*, **81**: 360–367.

Panji M and Ansari B (2017b), "Transient SH-Wave Scattering by the Lined Tunnels Embedded in an Elastic Half-Plane," *Engineering Analysis with Boundary Elements*, **84**: 220–230.

Panji M, Asgari MJ and Tavousi TSh (2011), "Evaluation of Effective Parameters on the Underground Tunnel Stability Using BEM," *Journal of Structural Engineering and Geotechnics*, **1**(2): 29–37.

Panji M, Kamalian M, Asgari Marnani J and Jafari MK (2013), "Transient Analysis of Wave Propagation Problems by Half-Plane BEM," *Geophysical Journal International*, **194**(3): 1849–1865.

Panji M, Kamalian M, Asgari Marnani J and Jafari MK (2014a), "Analyzing Seismic Convex Topographies by a Half-Plane Time Domain BEM," *Geophysical Journal International*, **197**(1): 591–607.

Panji M, Kamalian M, Asgari Marnani J and Jafari MK (2014b), "Antiplane Seismic Response from Semi-Sine Shaped Valley above Embedded Truncated Circular Cavity: A Time domain Half-Plane BEM," *International Journal of Civil Engineering*, **12**(2): 160–173.

Panji M, Koohsari H, Adampira M, Alielahi H and Asgari MJ (2016), "Stability Analysis of Hallow Tunnels Subjected to Eccentric Loads by a Boundary Element Method," *Journal of Rock Mechanics and Geotechnical Engineering*, **8**(2016): 480–488.

Panji M, Mojtabazadeh-Hasanlouei S and Yasemi F (2020), "A Half-Plane Time-Domain BEM for SH-Wave Scattering by a Subsurface Inclusion," *Computers & Geosciences*, **134**: 1–19.

Panji M and Mojtabazadeh-Hasanlouei S (2020), "Transient Response of Irregular Surface by Periodically Distributed Semi-Sine Shaped Valleys: Incident SH-Waves," *Journal of Earthquake and Tsunami*, **14**(1): 1–34.

Panji M and Mojtabazadeh-Hasanlouyi S (2018), "Time-History Response on the Surface by Regularly Distributed Enormous Embedded Cavity: Incident SH-Waves," *Earthquake Science*, **31**: 137–153.

Qiu F and Liu D (2005), "Antiplane Response of Isosceles Triangular Hill to Incident SH Waves," *Earthquake Engineering and Engineering Vibration*, **4**(1): 37–46.

Ricker N (1953), "The Form and Laws of Propagation of Seismic Wavelets," *Geophysics*, **18**(1): 10–40.

Sabina FJ and Willis JR (1975), "Scattering of SH Waves by a Rough Half-Space of Arbitrary Slope," *Geophysics. J. R. Astr. Soc.*, **42**(2): 685–703.

Sanchez-Sesma FJ, Herrera I and Aviles J (1982), "A Boundary Method for Elastic Wave Diffraction: Application to Scattering of SH Waves by Surface Irregularities," *Bulletin of the Seismological Society of America*, **72**(2): 473–49.

Sanchez-Sesma FJ, Palencia VJ and Luzon F (2002), "Estimation of Local Site Effects During Earthquakes: An Overview," *ISET Journal of Earthquake*, **39**(3): 167–193.

Sanchez-Sesma FJ and Esquivel JA (1979), "Ground Motion on Alluvial Valleys Under Incident Plane SH Waves," *Bull. Seism. Soc. Am*., **69**(4): 1107–1120.

Sanchez-Sesma FJ and Rosenblueth E (1979), "Ground Motion at Canyons of Arbitrary Shape Under Incident SH Waves," *Earthq. Eng. Struct. Dyn.*, **7**: 441–450.

Sills LB (1978), "Scattering of Horizontally-Polarized Shear Waves by Surface Irregularities," *Geophysical Journal International*, **54**(2): 319–348.

Smith WD (1975), "The Application of Finite Element Analysis to Body Wave Propagation Problems," *Geophysical Journal International*, **42**: 747–768.

Takemiya H and Fujiwara A (1994), "SH-Wave Scattering and Propagation Analysis at Irregular Sites by Time Domain BEM," *Bulletin of the Seismological Society of America*, **84**(5): 1443–1455.

Tsaur D and Chang K (2009), "Scattering and Focusing of SH Waves by a Convex Circular-Arc Topography," *Geophysical Journal International*, **177**(1): 222–234.

Virieux J (1984), "SH-Wave Propagation in Heterogeneous Media: Velocity-Stress Finite-Difference Method," *Geophysics*, **49**(2): 1933–1957.

Wong HL and Jennings PC (1975), "Effects of Canyon Topography on Strong Ground Motion," *Bull. Seism. Soc. Am.*, **65**(5): 1239–1257.

Wang G and Liu D (2002), "Scattering of SH-Wave by Multiple Circular Cavities in Half Space," *Earthquake Engineering and Engineering Vibration*, **1**(1): 36–44.

Yang Z, Xu H, Hei B and Zhang J (2014), "Antiplane Response of Two Scalene Triangular Hills and a Semi-Cylindrical Canyon by Incident SH-Waves," *Earthquake Engineering and Engineering Vibration*, **13**(4): 569–581.

Yuan XM and Liao ZP (1996a), "Surface Motion of a Cylindrical Hill of Circular Arc Cross Section for Incident Plane SH Waves," *Soil Dynamics and Earthquake Engineering*, **15**(3): 189–199.

Yuan XM and Liao ZP (1996b), "Scattering of Plane SH Waves by a Cylindrical Hill of Circular- Arc Cross Section," *Journal of Earthquake Engineering and Engineering Vibration*, **16**(2): 141–152.

Yuan X and Men FL (1992), "Scattering of Plane SH Waves by a Semi-Cylindrical Hill," *Earthquake Engineering and Structural Dynamics*, **21**(12): 1091–1098.

Zhang N, Gao Y, Li D, Wu Y and Zhang F (2012), "Scattering of SH Waves Induced by a Symmetrical V-Shaped Canyon: A Unified Analytical Solution," *Earthquake Engineering and Engineering Vibration*, **11**(1): 445–460.

Zhang N, Gao Y, Yang J and Xu Ch (2015), "An Analytical Solution to the Scattering of Cylindrical SH Waves by a Partially Filled Semi-Circular Alluvial Valley: Near-Source Site Effects," *Earthquake Engineering and Engineering Vibration*, **14**: 189–201.

Zhang N, Gao Y, Wu Y and Zhang F (2018), "A Note on Near-Field Site Amplification Effects of Ground Motion from a Radially Inhomogeneous Valley," *Earthquake Engineering and Engineering Vibration*, **17**(4): 707–718.

Zhou H and Chen X (2006), "A New Approach to Simulate Scattering of SH Waves by an Irregular Topography," *Geophysical Journal International*, **164**(2): 449–459.